

# 1    **The Portuguese man-of-war: Adrift in the North Atlantic Ocean**

2    Luis Ferrer<sup>a,\*</sup>, Yolanda Sagarminaga<sup>a</sup>, Ángel Borja<sup>a</sup>, Mikel Nogues<sup>b</sup>, María José Alegre<sup>c</sup>, María Santos<sup>a</sup>,  
3    Guillermo Boyra<sup>a</sup>, Paula Álvarez<sup>a</sup>, Beatriz Beldarrain<sup>a</sup>, Raúl Castro<sup>a</sup>, Gaizka Bidegain<sup>a</sup>, Manuel  
4    González<sup>a</sup>, Marta Revilla<sup>a</sup>, Izaskun Zorita<sup>a</sup>, Oihana Solaun<sup>a</sup>, Almudena Fontán<sup>a</sup>, José Germán Rodríguez<sup>a</sup>

5    <sup>a</sup>*AZTI, Marine Research, Basque Research and Technology Alliance (BRTA), Herrera Kaia, Portualdea*  
6    *z/g, 20110 Pasaia, Spain*

7    <sup>b</sup>*Department of Security, Basque Government, Donostia-San Sebastián, 1, 01010 Vitoria-Gasteiz, Spain*

8    <sup>c</sup>*Osakidetza, Altza-Roteta Health Centre, Paseo Larratxo, 95, 20017 Donostia-San Sebastián, Spain*

9

10

11    \* Corresponding author. AZTI, Marine Research, Basque Research and Technology Alliance (BRTA),  
12    Herrera Kaia, Portualdea z/g, 20110 Pasaia, Spain.

13    *E-mail address:* lferrer@azti.es (L. Ferrer).

14

15    **Abstract:** On 11 February 2014, dozens of Portuguese man-of-war specimens were washed ashore along  
16    the entire stretch of Patos Beach (northwestern Spain). Here we performed both field experiments and  
17    numerical simulations to estimate the possible trajectories and region of origin of this swarm. On the one  
18    hand, our field experiments confirm the need to consider the main characteristics of an organism when  
19    predicting its drift. On the other hand, the numerical simulations show that this swarm originated in the  
20    open North Atlantic Ocean. The drift of the swarm was controlled by the succession of storms that hit the  
21    coasts of Western Europe in the winter of 2013–14. Our findings also suggest that most of the individuals  
22    of the swarm were right-handed.

23

## 24    **1. Introduction**

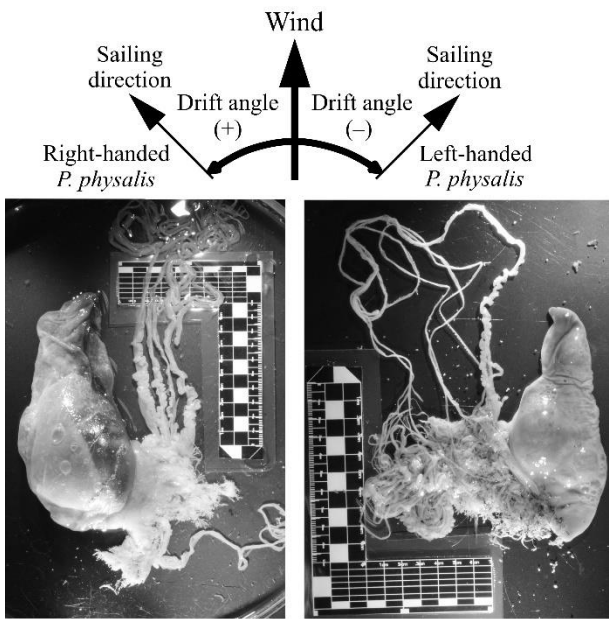
25        In the winter of 2013–14, a succession of destructive storms hit the coasts of Western Europe  
26    leading to record rainfall and flooding in many regions (Castelle et al., 2015; Kendon and McCarthy,  
27    2015; Sibley et al., 2015; Thompson et al., 2017). This had a considerable impact on infrastructure and  
28    businesses. During this severe winter, the northwestern coast of Spain experienced repeated intense  
29    rainfall events, strong winds, high waves and a large number of strandings of marine animals. Although  
30    many strandings in coastal areas around the world end up as unsolved cases, scientists have no shortage of  
31    suspected causes, including bycatch, disease, poisoning, injuries, parasites, malnutrition and storms (e.g.  
32    Arbelo et al., 2013; Truchon et al., 2013; Morley et al., 2016; Louzao et al., 2019; Dudhat et al., 2022).

33        On 11 February 2014, dozens of Portuguese man-of-war specimens (hereafter referred to as the 2014  
34    PMW swarm) were washed ashore along the entire stretch of Patos Beach. This beach is located on the coast  
35    of Galicia (northwestern Spain). The Portuguese man-of-war (*Physalia physalis*) is a wind-propelled

jellyfish-like animal that lives in warm tropical and subtropical waters (Totton and Mackie, 1960; Kennedy, 1972; Bardi and Marques, 2007; Mapstone, 2014; Ferrer et al., 2015; Munro et al., 2019). Therefore, the 2014 PMW swarm probably originated in the open North Atlantic Ocean and its drift was controlled by the succession of low-pressure systems mentioned above.

The Portuguese man-of-war is a peculiar-looking colony of specialized polyps. The gonozooids and gastrozooids are used for reproduction and feeding, respectively, while the dactylozooids are used for catching prey and self-defense. The pneumatophore is a gas-filled sail-like float that allows the Portuguese man-of-war to live at the air–water interface of the sea. Large quantities of Portuguese man-of-war specimens in coastal regions have forced beaches to close and left thousands of bathers nursing painful stings. The treatment of these stings has been discussed by several researchers (e.g. Loten et al., 2006; Cegolon et al., 2013; Wilcox and Yanagihara, 2016).

The Portuguese man-of-war occurs in two forms (i.e. dimorphism) which are mirror images of one another, but otherwise identical. Some observations reveal that, under the influence of the wind, one form (left-handed) moves to the right of the downwind direction and the other (right-handed) to the left (Totton and Mackie, 1956, 1960; Woodcock, 1956, 1971, 1997; Bieri, 1959; Savilov, 1961; Shannon and Chapman, 1983). The sailing directions of these two forms are shown in Fig. 1. More recently, Ferrer and González (2021) ran computer simulations to demonstrate that the drift of left-handed individuals can be significantly different from that of right-handed individuals.



Portuguese man-of-war

**Fig. 1.** Sailing directions of right- and left-handed *P. physalis*.

Although much work has been devoted to the Portuguese man-of-war to date, more studies need to be conducted to ascertain the effect of dimorphism on the drift of this colonial organism. Unfortunately, there is no information on whether the individuals of the 2014 PMW swarm were right- or left-handed. For this reason, the aim of the research presented here was to estimate the possible trajectories (routes) and region of origin of the 2014 PMW swarm. To do this, we performed both field experiments and numerical simulations.

## 2. Methods

At present, social media and digital newspapers are two of the main sources of information for the public and many researchers. Therefore, the first step of the study was to collect the existing information on the 2014 PMW swarm from these two sources. After reviewing this information in detail and confirming the occurrence of this event, we decided to conduct both field experiments and numerical simulations to achieve the initially proposed goal of studying the drift of the 2014 PMW swarm.

We conducted two field experiments to obtain information on the drift of small low-density objects. In the first experiment, we designed and made the two forms of the Portuguese man-of-war (i.e. right- and left-handed individuals). We used polyurethane foam and cables to simulate the float and tentacles (mass and volume, respectively: 30 g and 144 mL) of the Portuguese man-of-war (see Fig. 2). We repeatedly released the designed prototypes in the waters of the Bay of La Concha and Taurán Beach, located on the coast of the Basque Country and Asturias, respectively (northern Spain). We also performed the same in a small plastic box (58 cm x 38 cm x 16 cm in length x width x height) filled with water. The aim of this first experiment was to determine whether there were statistically significant differences in the drifts of the designed prototypes in different wind conditions.

In the second experiment, we used satellite-tracked surface drifting buoys called marmokas. These buoys, with cylindrical shape (184 g and 775 mL), were designed to be at the sea surface and obtain high-resolution trajectories. The components of these buoys are shown in Fig. 2. Each buoy consists of a wide mouth and high-density polyethylene jar (with lid and insert plug) containing a SPOT Trace device ([www.findmespot.com](http://www.findmespot.com)). Almost 77% of the buoy volume is out of the water and under the influence of the wind.

The SPOT Trace is a small tracking device (88 g and 75 mL) that provides satellite-based messaging capabilities to track anything, anytime, with extensive coverage around the world. This device allows to select the rate at which GPS locations are sent. In our case, we obtained GPS locations every hour. In total, we released 27 surface drifting buoys in the open waters of the Bay of Biscay using ships of opportunity and research vessels. The drift periods and the initial and final GPS locations of these buoys are listed in Table 1. The aim of this second experiment was to obtain a large database of buoy trajectories to help understand and explain the possible drift of the Portuguese man-of-war.



**Fig. 2.** Prototypes of right- and left-handed *P. physalis* (top) and components of the satellite-tracked surface drifting buoys used in this study (bottom).

To estimate the possible routes and region of origin of the 2014 PMW swarm, we used the trajectories of the buoys listed in Table 1 and the Sediment, Oil spill and Fish Tracking model (SOFT). This model is an easy-to-use and computationally efficient Lagrangian particle tracking tool. Although it was

initially developed to simulate the dispersal of marine eggs and larvae in the Bay of Biscay (Ferrer et al., 2004), it can now be used to simulate other types of dispersal as well. Since 2017, SOFT includes the following equation to estimate the drift of a Portuguese man-of-war:

$$\mathbf{U}_D = C_D \mathbf{U}_{W,\theta} = C_D U_{W,\theta} + C_D V_{W,\theta} \quad (1)$$

where  $\mathbf{U}_D = (U_D, V_D)$  is the drift velocity vector,  $C_D$  is a wind drag coefficient and  $\mathbf{U}_{W,\theta} = (U_{W,\theta}, V_{W,\theta})$  is the wind velocity vector at 10 m height rotated a drift angle  $\theta$  about the wind direction. The direction of rotation is clockwise if  $\theta$  is negative (for left-handed individuals) and anticlockwise if  $\theta$  is positive (for right-handed individuals). In the model, the method used for the movement of particles (i.e. sediments, oil spills, eggs and larvae, jellyfish, Portuguese man-of-war specimens, etc.) is based on the fourth-order Runge–Kutta scheme.

**Table 1**

Drift periods and initial and final GPS locations of the 27 satellite-tracked surface drifting buoys used in this study.

Buoy ID	Initial and final dates (day/month/year) and times (UTC)	Initial and final GPS locations
20150517A	17/05/2015 09:54:22–13/06/2015 12:13:01	45.45° N, 4.21° W–43.44° N, 4.06° W
20150517B	17/05/2015 10:58:54–16/06/2015 09:44:36	45.63° N, 4.21° W–43.44° N, 2.95° W
20150926	26/09/2015 00:41:54–25/10/2015 00:26:37	45.88° N, 4.69° W–46.02° N, 8.59° W
20151025	25/10/2015 19:19:36–06/11/2015 11:38:34	46.22° N, 8.61° W–48.31° N, 8.81° W
20160321A	21/03/2016 02:48:12–04/04/2016 23:52:05	46.26° N, 4.28° W–46.47° N, 3.1° W
20160321B	21/03/2016 05:14:35–11/04/2016 05:02:25	46.25° N, 4.75° W–46.23° N, 1.87° W
20160321C	21/03/2016 08:28:59–11/04/2016 05:50:36	46.25° N, 5.26° W–46.62° N, 2.68° W
20160321D	21/03/2016 22:17:58–05/04/2016 00:19:53	46.76° N, 5.77° W–47.65° N, 3.51° W
20160322	22/03/2016 02:25:22–04/04/2016 00:10:08	46.77° N, 5.26° W–47.79° N, 3.83° W
20160519A	19/05/2016 07:13:35–16/06/2016 20:39:23	45.87° N, 4.21° W–43.79° N, 1.42° W
20160519B	19/05/2016 09:08:05–28/06/2016 10:41:23	46.12° N, 4.38° W–43.84° N, 2.01° W
20160709	09/07/2016 07:07:06–01/08/2016 12:12:53	45° N, 3.36° W–43.55° N, 5.55° W
20160923	23/09/2016 15:35:06–13/11/2016 19:14:07	45.78° N, 4.2° W–44.64° N, 8.7° W
20170517	17/05/2017 13:30:07–30/06/2017 14:17:28	45.87° N, 3.71° W–43.49° N, 3.83° W
20180222	22/02/2018 21:58:52–04/04/2018 08:57:26	45.5° N, 4.03° W–46.63° N, 1.89° W
20180224	24/02/2018 11:20:40–31/03/2018 23:42:58	45.5° N, 4.38° W–46.53° N, 1.83° W
20180225	25/02/2018 03:18:37–04/04/2018 06:25:25	45.51° N, 4.19° W–46.65° N, 1.91° W
20180226	26/02/2018 23:17:06–14/03/2018 23:50:23	45.5° N, 3.86° W–47.49° N, 2.83° W
20180515	15/05/2018 03:51:09–21/05/2018 10:14:56	44.86° N, 2.84° W–44.23° N, 3.01° W
20190320	20/03/2019 15:56:58–24/04/2019 11:18:27	46.25° N, 4.18° W–45.72° N, 5.96° W
20190409	09/04/2019 15:32:57–12/04/2019 09:17:23	46° N, 4.01° W–45.75° N, 4.21° W

20190418	18/04/2019 22:14:07–27/04/2019 20:23:26	46° N, 4.02° W–46.13° N, 2.75° W
20200918	18/09/2020 16:06:42–26/09/2020 16:27:57	44.67° N, 3.04° W–44.2° N, 1.3° W
20210513	13/05/2021 08:10:26–23/05/2021 07:54:59	45.62° N, 4.13° W–45.64° N, 1.1° W
20210919	19/09/2021 20:06:19–25/11/2021 00:57:35	45.77° N, 4.17° W–43.46° N, 3.95° W
20210920	20/09/2021 12:16:23–27/11/2021 05:42:57	45.93° N, 4.55° W–43.44° N, 4.1° W
20220515	15/05/2022 11:20:40–13/06/2022 18:02:27	45.13° N, 3.63° W–43.58° N, 5.74° W

The methodology applied was as follows. First, we obtained a large number of two-day trajectories using the buoy trajectories. If a buoy trajectory has  $N$  hourly GPS locations (where  $N > 48$ ), we can obtain  $N - 48$  two-day trajectories. That is, two-day trajectories 1 and 2 would have the GPS locations from  $t = 0$  h to  $t = 48$  h, and from  $t = 1$  h to  $t = 49$  h, respectively. Therefore, two-day trajectory  $i$  would have the GPS locations from  $t = (i - 1)$  h to  $t = (i + 47)$  h. For example, we can obtain four different two-day trajectories from the trajectory shown at the top of Fig. 3. Using this methodology and the trajectories of the buoys listed in Table 1, we obtained 16,292 two-day trajectories.

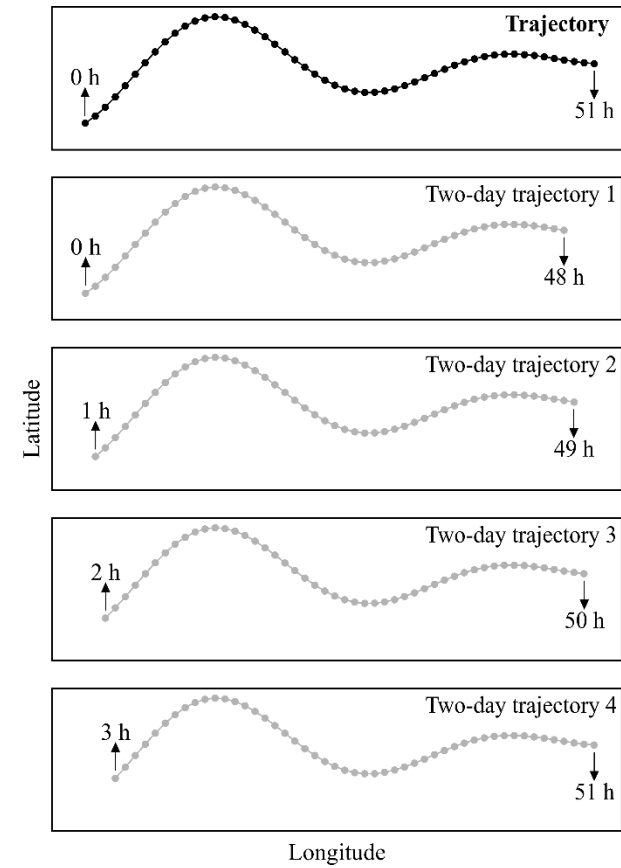


**Fig. 3.** Two-day trajectories obtained from an initial example trajectory.

Second, we used SOFT to simulate the two-day trajectories obtained in the first step. In our numerical simulations with SOFT, we used Eq. (1) with the hourly wind fields provided by the operational

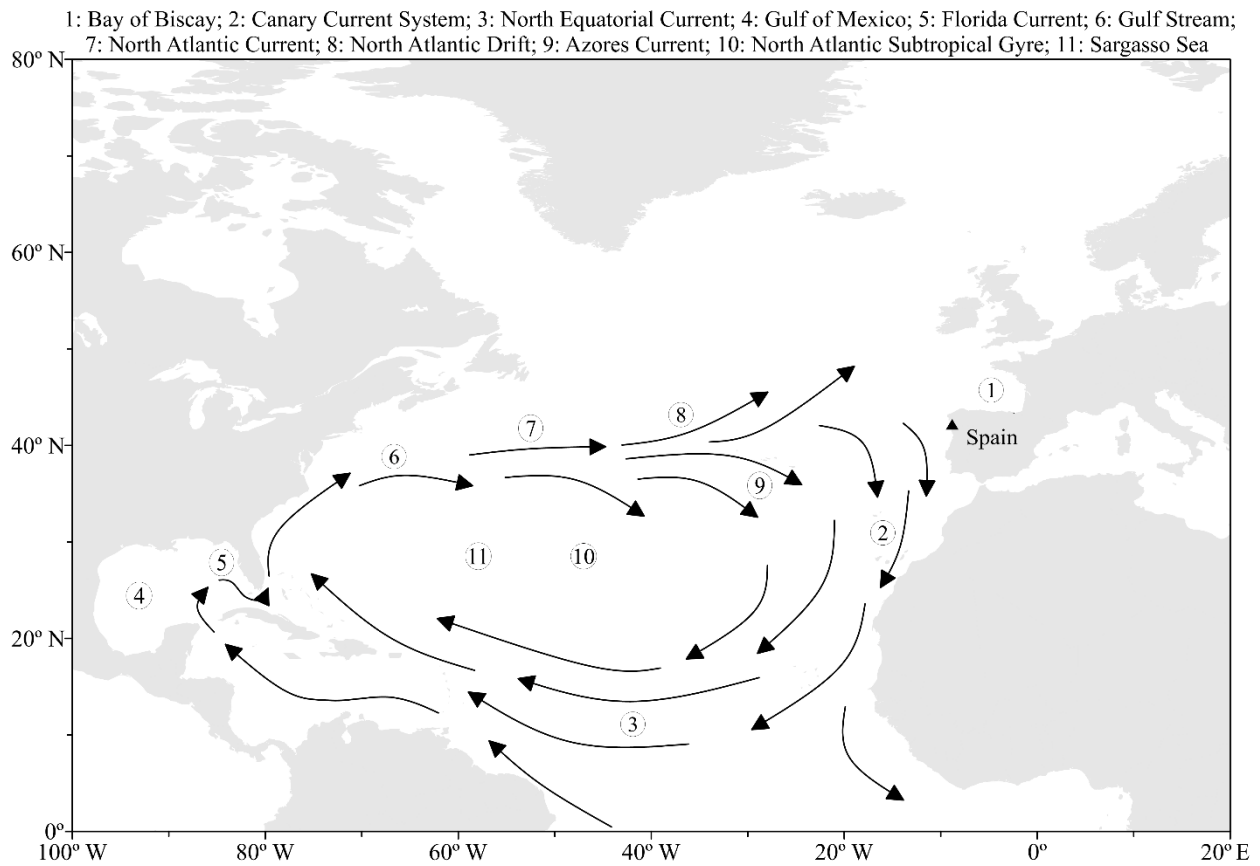
forecasting system developed by MeteoGalicia (Meteorological Agency of Galicia). These wind fields, with a spatial resolution of 12 km, were obtained using the Weather Research and Forecasting model (WRF). A detailed description of this model can be found in Skamarock et al. (2021). The time step used in the numerical simulations with SOFT was 10 s.

We also used 14 values for  $C_D$  (from 0.005 to 0.07 with an increment of 0.005) and 21 for  $\theta$  (from  $-50^\circ$  to  $+50^\circ$  with an increment of  $+5^\circ$ ). In total, we ran SOFT 294 (i.e. 14 x 21) times to simulate each two-day trajectory. The aim of these simulations was to find the values of  $C_D$  and  $\theta$  that best fit each two-day trajectory and then use these values to estimate the drift of the Portuguese man-of-war. To do so, we estimated the non-dimensional index  $s$  (normalized cumulative Lagrangian separation) proposed by Liu and Weisberg (2011). Note that the smaller the  $s$  value, the better the performance of the model, and that  $s = 0$  implies a perfect fit between observations and simulations.

And third, we ran SOFT backwards in time to estimate the most likely routes (or trajectories) and region of origin of the 2014 PMW swarm in the North Atlantic Ocean. The initial location of this swarm in the simulations (about 10 km off the coast of Galicia) is shown in Fig. 4. The simulated swarm was moved backwards in time using SOFT for 163 days (i.e. from 11 February 2014 to 1 September 2013, both dates at 12:00 UTC), assuming that reproduction occurred between summer and autumn. Here we used the best-fit  $C_D$  values obtained in the second step and hourly wind fields from the ERA5 global reanalysis (Hersbach et al., 2018). This database, with a spatial resolution of 31 km, was produced by the European Centre for Medium-Range Weather Forecasts (ECMWF).

### 3. Results

In the first experiment, we released the designed PMW prototypes in the waters of the Bay of La Concha and Taurán Beach, and in a small plastic box filled with water. The drifts of these prototypes were visually inspected for several hours on different days in 2023. Our observations confirmed that the designed prototypes drifted differently. Under the influence of light to moderate winds, left-handed prototypes drifted to the right of the downwind direction, while right-handed prototypes drifted to the left of the downwind direction. This result is consistent with previous observations (see the Introduction section) and confirms the need to consider the main characteristics of an organism when predicting its drift.



156

157

158

159

160

161

162

163

164

165

166

167

168

**Fig. 4.** General surface ocean circulation in the North Atlantic Subtropical Gyre. The black triangle indicates the initial location (42.2° N, 8.9° W) of the 2014 PMW swarm in the SOFT simulations where time ran backwards.

In the second experiment, we released 27 surface drifting buoys in the open waters of the Bay of Biscay between May 2015 and June 2022. The trajectories of four of these buoys and some speed statistics (range, mean and standard deviation) are shown in Fig. 5. These trajectories show the complexity of the drift of a small low-density object ( $\sim 0.24 \text{ g mL}^{-1}$ ) at the air–water interface of the sea. The maximum and mean speeds of the buoys listed in Table 1 were  $136 \text{ cms}^{-1}$  and  $35 \text{ cms}^{-1}$ , respectively, with a standard deviation of about  $17 \text{ cms}^{-1}$ . The drift of this type of buoy is very much controlled by the wind at the sea surface because most of the buoy is out of the water. On average, the drift of the buoys was from west-northwest to east-southeast.



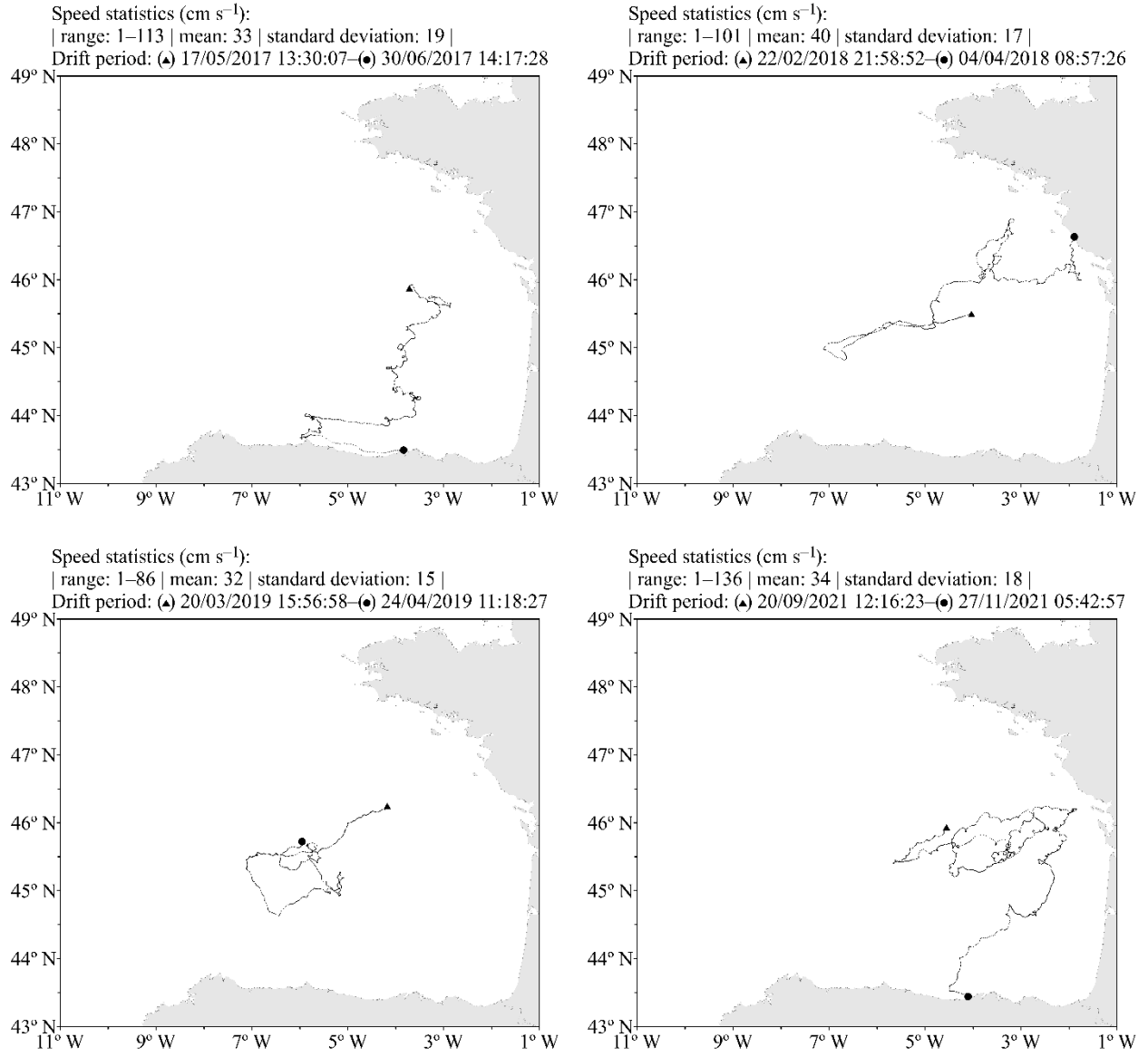


**Fig. 5.** Trajectories of four satellite-tracked surface drifting buoys (from top left to bottom right: 20170517, 20180222, 20190320 and 20210920). The black triangles and circles indicate the initial and final GPS locations of the buoys, respectively.

Using SOFT, we simulated the 16,292 two-day trajectories obtained from the buoy trajectories. From these simulations, we found the values of  $C_D$  and  $\theta$  that best fit each two-day trajectory. For each two-day trajectory, we also estimated the non-dimensional index  $s$ , the mean and maximum errors, and the error at the end of the trajectory. Our simulations show that  $s$  ranged from 0.03 to 0.78, while the mean errors ranged from 0.93 km to 23 km.

We found that 50% of the two-day trajectories had  $s \leq 0.1$  (i.e. mean error  $\leq 6.1$  km). The mean values of  $C_D$  and  $\theta$  for these two-day trajectories were 0.04 and  $-13^\circ$ , respectively. Given these results, we decided to use three different values for  $C_D$  (0.02, 0.04 and 0.06) in the simulations to estimate the drift of

the 2014 PMW swarm. The use of these values allowed us to identify differences in the drift of the swarm. In the simulations, we also used the 21 values for  $\theta$  given in the Methods section.

The trajectories of the 2014 PMW swarm obtained after running SOFT backwards in time for 163 days are displayed in Figs. 6–8. The trajectories obtained using negative (positive) drift angles correspond to left-handed (right-handed) individuals. The end points of these trajectories on 1 September 2013 are the estimated locations of our swarm at the initial stage of development (i.e. at the age of 0 days). We used the end points located in the open North Atlantic Ocean to approximately delimit the region of origin of the 2014 swarm. The end points located on the coast were discarded as possible points of origin.

On the one hand, the simulations carried out with a  $C_D$  value equal to 0.04 (Fig. 6) show that the region of origin of the 2014 PMW swarm was located in the open North Atlantic Ocean. According to the model, with negative drift angles this region would be located above  $49.76^\circ$  N, while with positive drift angles it would be located below this latitude. Since we assume that the Portuguese man-of-war is an organism that lives in warm tropical and subtropical waters, our model results suggest that most of the individuals of the 2014 PMW swarm were probably right-handed (i.e. with positive drift angles). Therefore, the region of origin was probably located below  $49.76^\circ$  N. The possible routes of the swarm covered a large geographical area.

On the other hand, the simulations carried out with  $C_D$  values equal to 0.02 and 0.06 (Figs. 7 and 8) also show that the region of origin was located in the open North Atlantic Ocean. With a  $C_D$  value equal to 0.02, the model estimated that this region would be located closer to the coast of Galicia. As can be seen in Figs. 6–8, the trajectories obtained with SOFT using different drift angles become longer and more complex as the value of the wind drag coefficient increases. Therefore, the selection of an appropriate wind drag coefficient is crucial for a successful estimation of the region of origin.

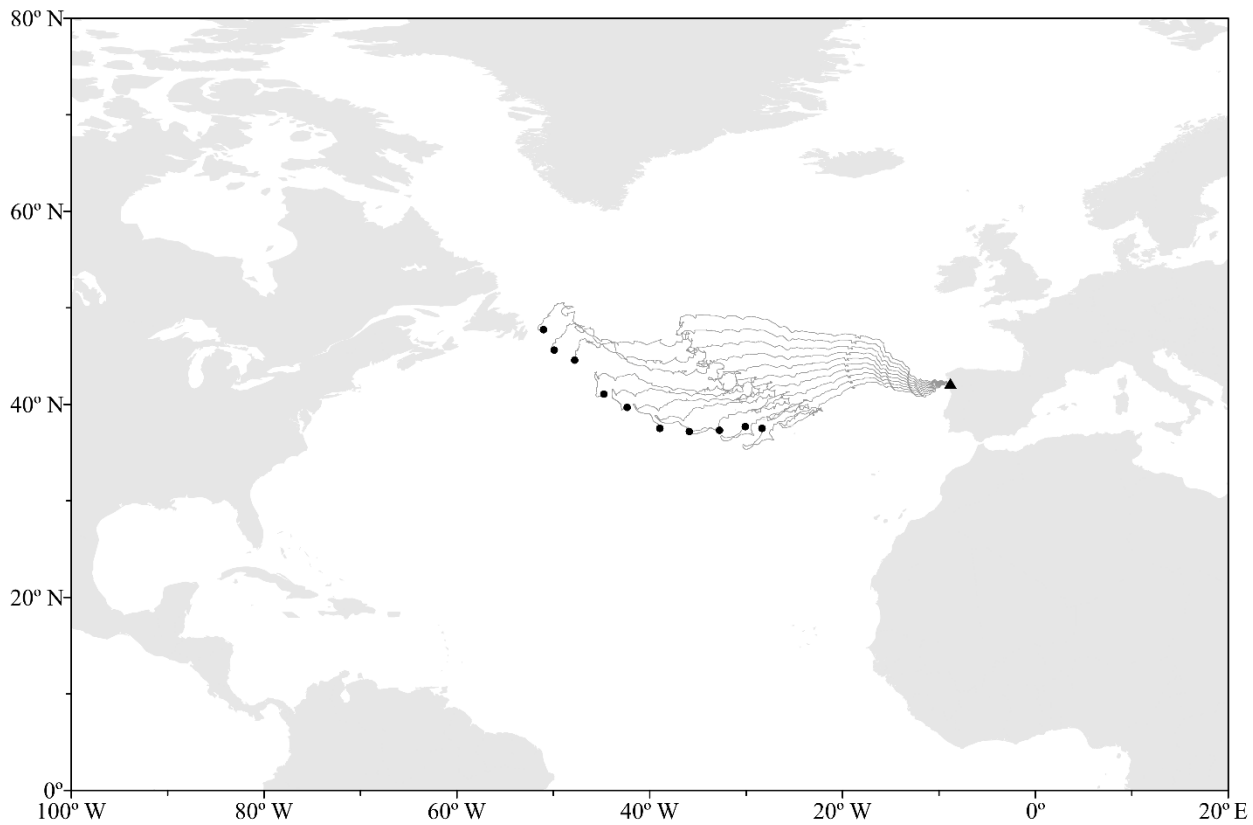
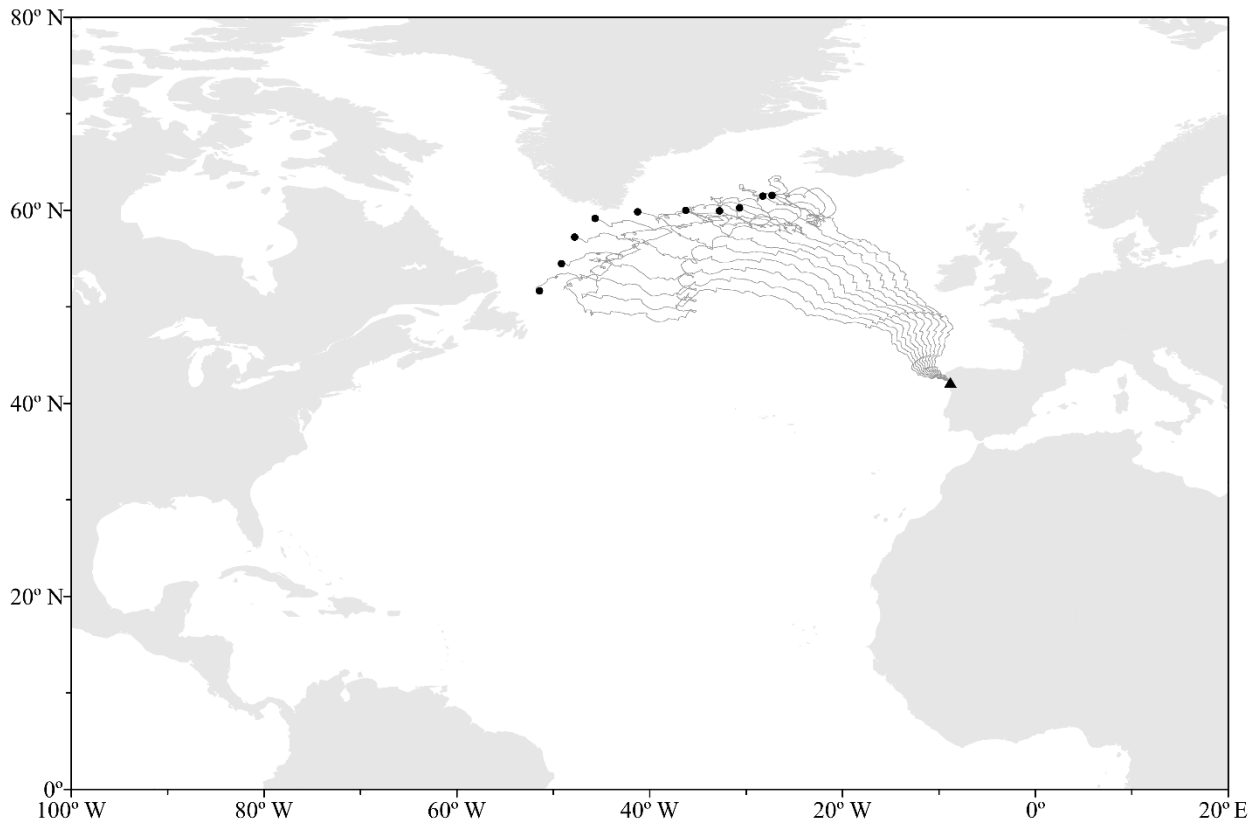


**Fig. 6.** Simulated trajectories of the 2014 PMW swarm (from 11 February 2014 to 1 September 2013, both dates at 12:00 UTC) obtained with SOFT using a wind drag coefficient of 0.04 and negative and positive drift angles (top and bottom, respectively). The black triangle and circles indicate the initial and final locations of the swarm in the SOFT simulations, respectively.

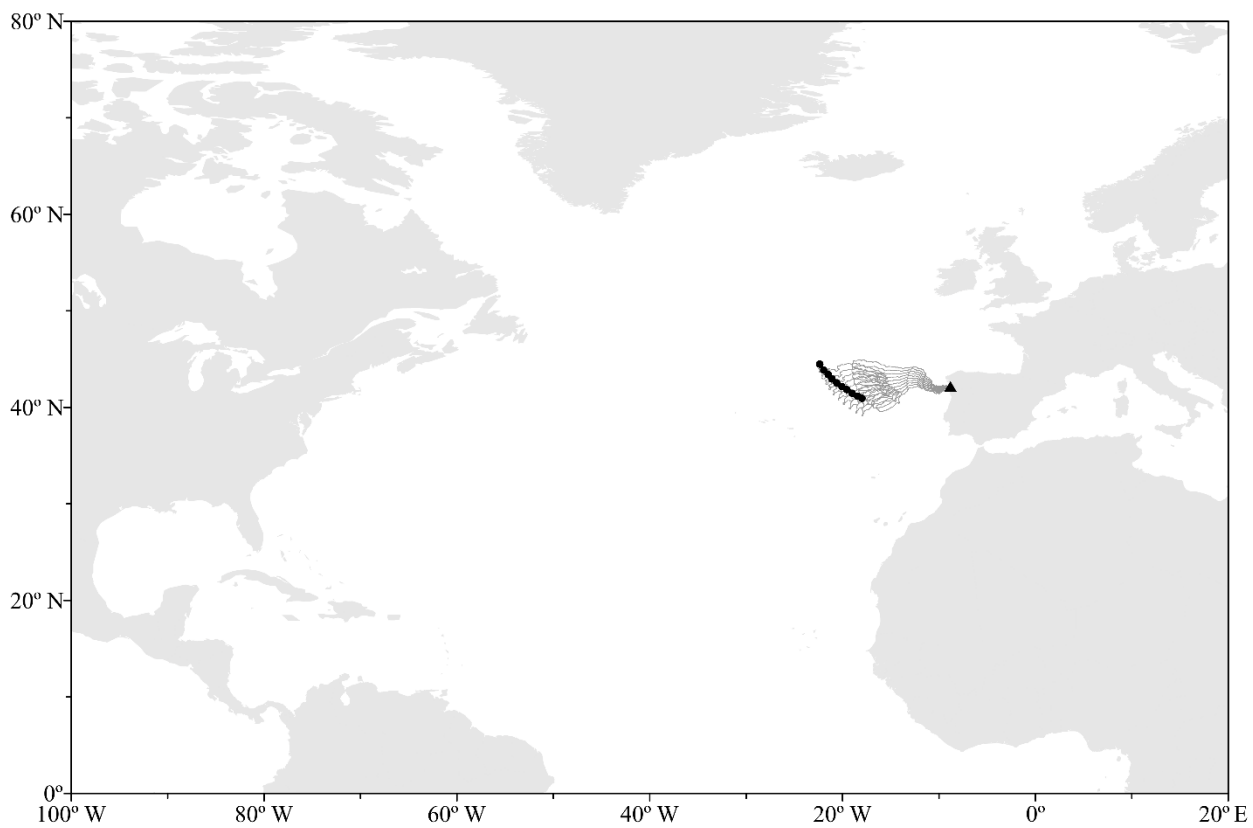
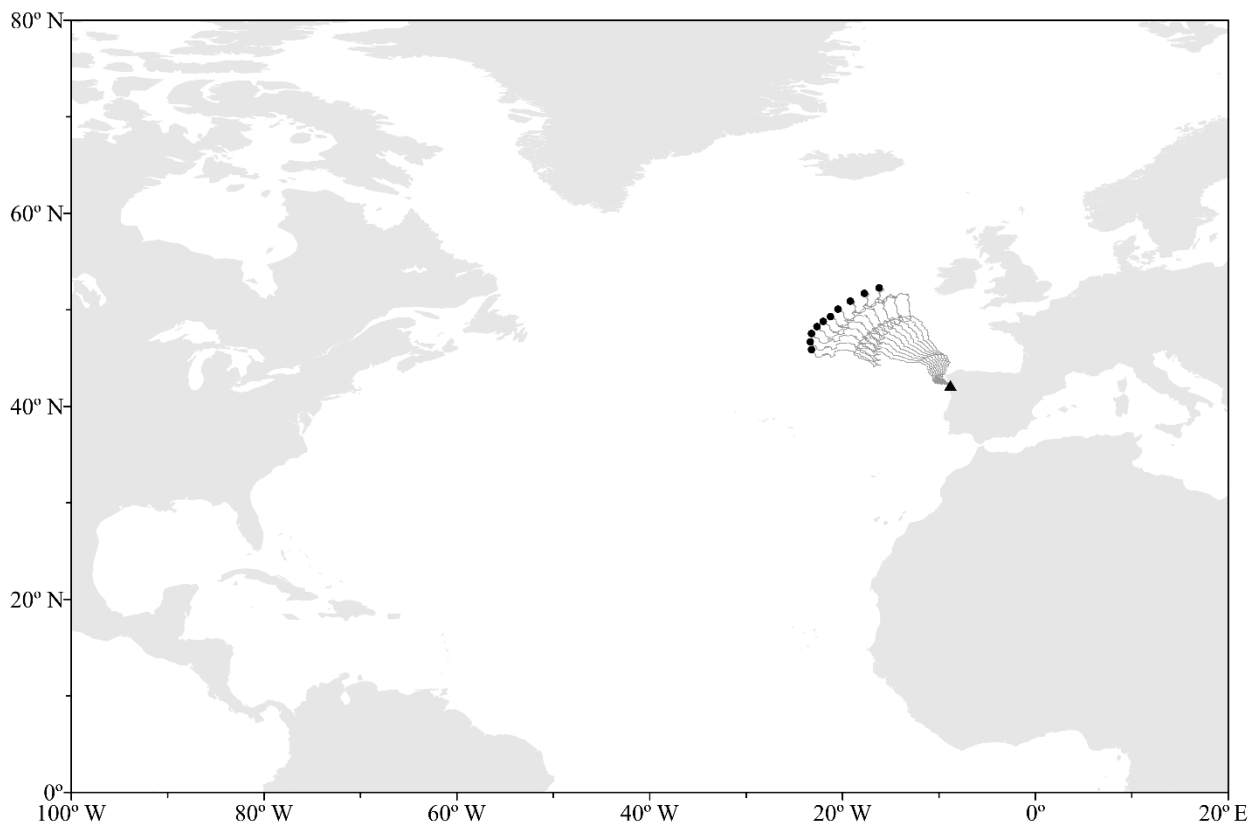


**Fig. 7.** As in Fig. 6, but using a wind drag coefficient of 0.02.

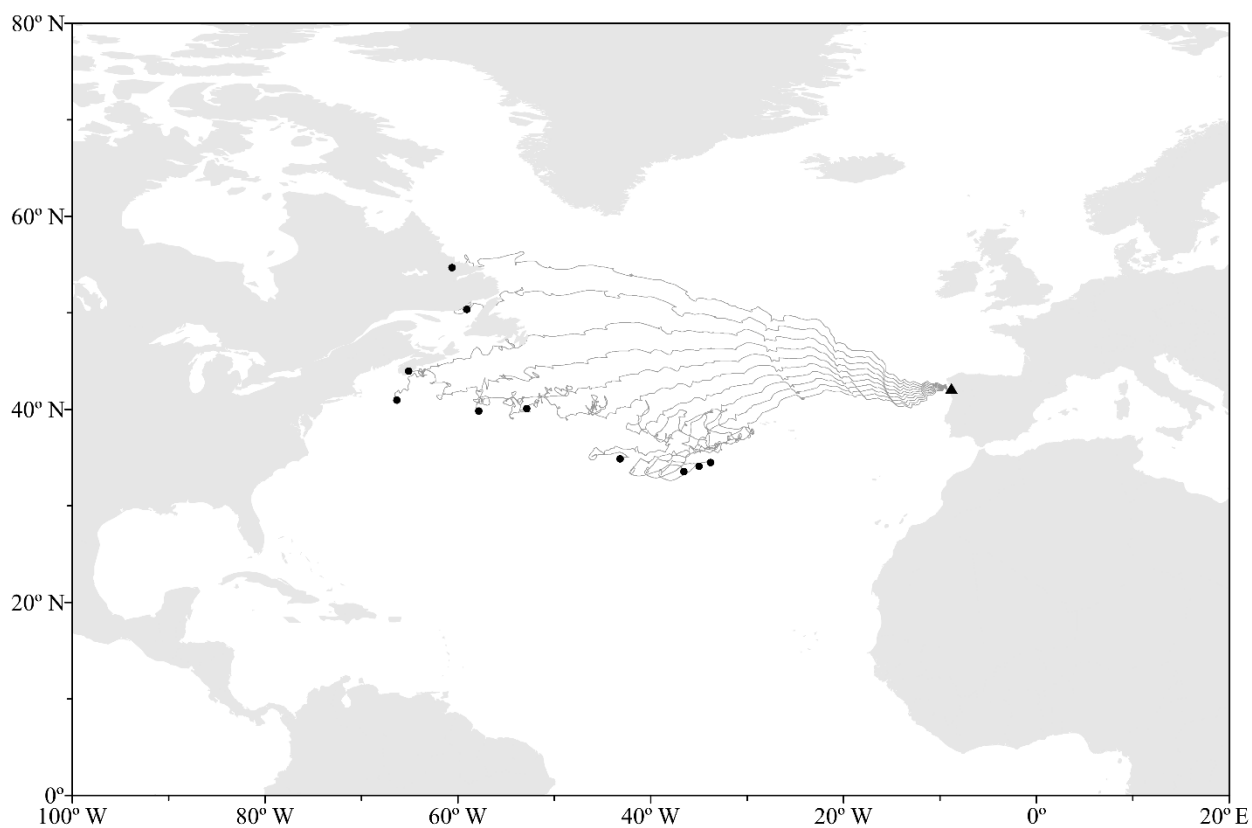
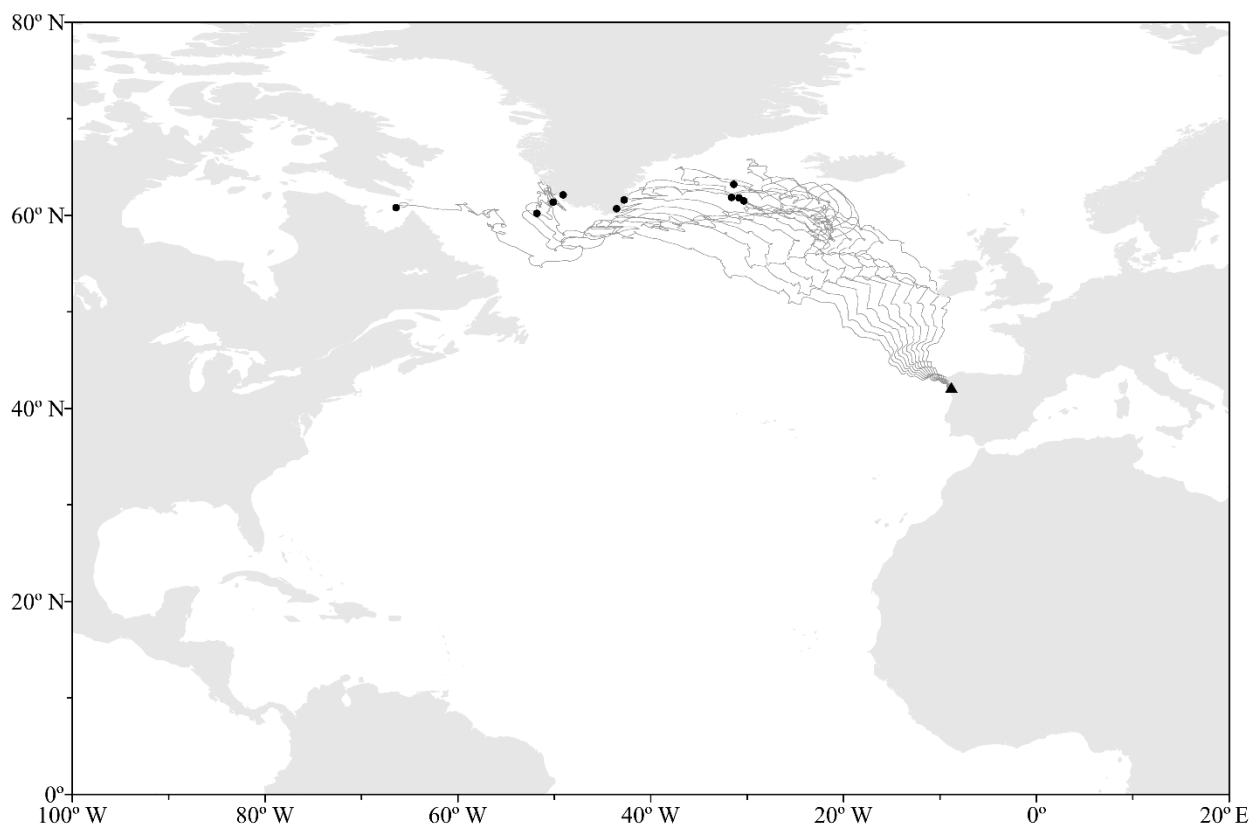


**Fig. 8.** As in Fig. 6, but using a wind drag coefficient of 0.06.

## 4. Discussion

Following the suggestion of Ferrer et al. (2015), here we used a simple model based only on wind information to investigate the most likely region of origin as well as the routes of the 2014 PMW swarm. We first designed and made the two forms of the Portuguese man-of-war and small surface drifting buoys. We then conducted field experiments with the designed prototypes and buoys. Finally, we simulated the trajectories of 27 surface drifting buoys and used the results obtained with the model to simulate the drift of the 2014 PMW swarm.

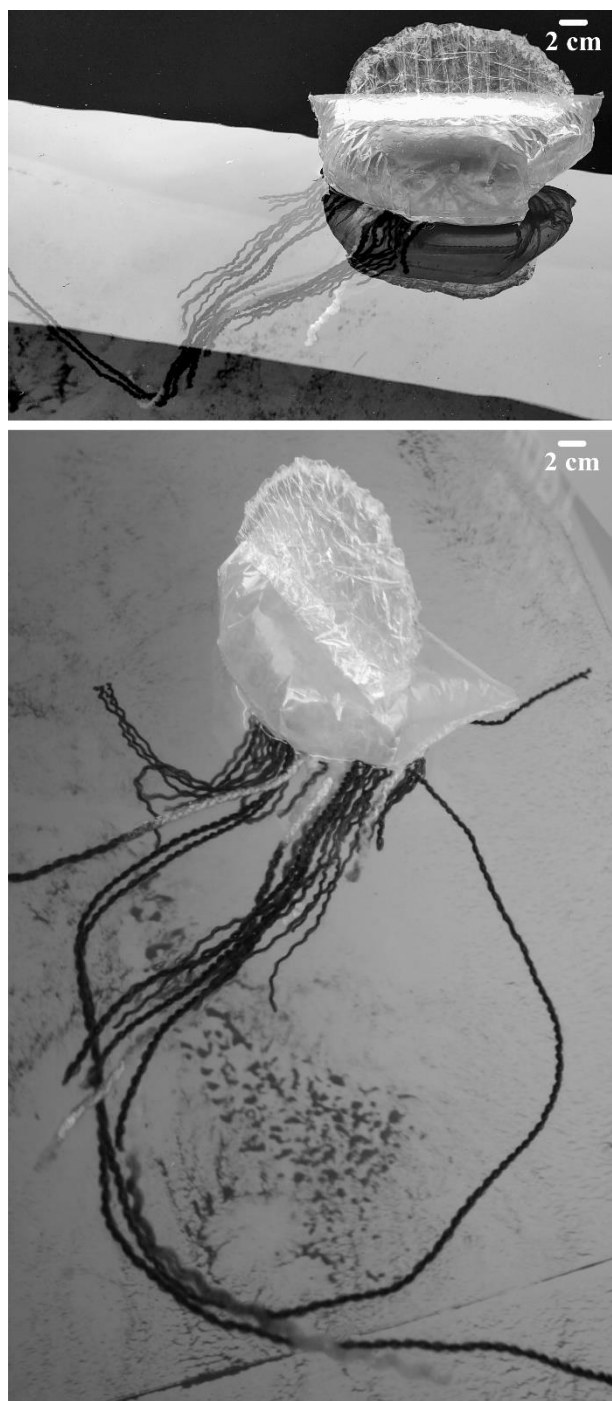
Many researchers have confirmed that the wind at the sea surface plays a key role in the drift of the Portuguese man-of-war (e.g. Orton, 1913; Wilson, 1947; Totton and Mackie, 1956, 1960; Woodcock, 1956, 1971, 1997; Shannon and Chapman, 1983; Iosilevskii and Weihs, 2009; Prieto et al., 2015; Ferrer et al., 2015). The same is true for *Velella velella* (by-the-wind sailor), which is another dimorphic organism living at the air–water interface of the sea (Bieri, 1959; Francis, 1991). Prior to this work, we also designed and made prototypes of the two forms of this organism and performed field experiments.

The first conclusion we can draw from our research is that the prototypes and surface drifting buoys used here were of great help in modelling the drift of the Portuguese man-of-war. These Identified Floating Objects (IFOs) are part of the Surface Ocean Circulation Experiment (SOCE) we are currently conducting in the North Atlantic Ocean. The main objective of this experiment is to accurately predict the drift of small surface organisms and objects. We have recently designed and made new low-density prototypes ( $< 0.1 \text{ g mL}^{-1}$ ) using air bags for packaging and wool yarns. These prototypes are closer to reality than those in Fig. 2 (see Fig. 9).

The second conclusion of this study is that the region of origin of the 2014 PWM swarm was located in the open North Atlantic Ocean. Assuming that most of the individuals of the 2014 PMW swarm were probably right-handed, the region of origin predicted by the model was located in the northern part of the North Atlantic Subtropical Gyre (Fig. 4). This conclusion agrees with the results obtained by Ferrer and González (2021). These authors carried out numerical simulations to study an event that occurred along the Basque coast in August 2010.

A wind drag coefficient of around 0.04 may be appropriate for studies assessing the drift of small surface organisms, such as *P. physalis* and *V. velella*. However, it seems reasonable to expect both the wind

247 drag coefficient and the drift angle to vary with wind speed and over the lifespan of *P. physalis* and *V.*  
248 *velella*, because there will be a significant increase in the size of these organisms (Ferrer and Pastor, 2017;  
249 Ferrer and González, 2021).



250  
251 **Fig. 9.** Low-density prototypes of right- and left-handed *P. physalis* made from air bags for packaging and  
252 wool yarns.

253  
254 In our simulations of the 2014 PMW swarm, we did not use the mean value of the drift angle  
255 obtained from the analysis of the 27 surface drifting buoys ( $\sim -13^\circ$ ). This value should be used to correct the

drift angles of right- and left-handed individuals used in the simulations. For example, considering this value, a right-handed (left-handed) individual with an initial drift angle of  $+30^\circ$  ( $-30^\circ$ ) would have a drift angle of  $+17^\circ$  ( $-43^\circ$ ). The mean drift angle obtained from the buoys used here (symmetrical objects with a significant part of the volume out of the water) is far from the angle given by the classical Ekman theory. According to this theory, in the Northern Hemisphere the drift angle is  $-45^\circ$  (Ekman, 1905).

The general surface ocean circulation in the North Atlantic Subtropical Gyre is shown in Fig. 4. This idealized wind-driven circulation indicates that we should expect a west-to-east surface drift in the northern part of the North Atlantic Subtropical Gyre. The drift of the Portuguese man-of-war (dimorphic organism with a gas-filled sail-like float) is mainly controlled by the wind. Therefore, the sailing directions and trajectories of right- and left-handed individuals will depend on the drift angles relative to the wind direction that they can reach.

The winter of 2013–14 in Western Europe was characterised by many intense cyclones. In February 2014, windstorms Nadja, Okka, Petra, Qumaira, Ruth, Stephanie, Tini and Ulla brought heavy rainfall and strong winds (Priestley et al., 2017). If the presence of the Portuguese man-of-war had occurred in summer (as happened in 2010 or 2023), it would have caused a significant social and economic impact (Labadie et al., 2012; Canepa et al., 2020; Cavalcante et al., 2020; Macías et al., 2021; Maharani and Widiastuti, 2021).

## 5. Conclusions

Here we analysed the presence of a Portuguese man-of-war swarm on the coast of Galicia (northwestern Spain) in February 2014. Our findings suggest the following conclusions: (1) the swarm originated in the open North Atlantic Ocean; (2) the drift of the swarm was controlled by the succession of storms that hit the coasts of Western Europe in the winter of 2013–14; and (3) most of the individuals of the swarm were probably right-handed. We hope that these findings will inspire other researchers to address unresolved questions about the Portuguese man-of-war.

## Acknowledgements



283        We thank MeteoGalicia for sharing its data and Nagore Zaldúa-Mendizabal for providing  
284        photographic material. The ERA5 hourly data were downloaded from the Copernicus Climate Change  
285        Service (C3S) Climate Data Store (CDS). This research was partially supported by two projects funded by  
286        the European Union's Horizon Europe research programme: GES4SEAS (Achieving Good Environmental  
287        Status for maintaining ecosystem Services, by ASsessing integrated impacts of cumulative pressures, grant  
288        agreement no. 101059877, [www.ges4seas.eu](http://www.ges4seas.eu)) and OBAMA-NEXT (OBserving And MApping marine  
289        ecosystems – NEXT generation tools, grant agreement no. 101081642, [www.obama-next.eu](http://www.obama-next.eu)). This paper is  
290        contribution no. 1213 from AZTI, Marine Research, Basque Research and Technology Alliance (BRTA).

## 291     **References**

- 292     Arbelo, M., Espinosa de los Monteros, A., Herráez, P., Andrada, M., Sierra, E., Rodríguez, F., Jepson, P.D.,  
293     Fernández, A., 2013. Pathology and causes of death of stranded cetaceans in the Canary Islands  
294     (1999–2005). *Dis. Aquat. Org.* 103, 87–99. <https://doi.org/10.3354/dao02558>.
- 295     Bardi, J., Marques, A.C., 2007. Taxonomic redescription of the Portuguese man-of-war, *Physalia physalis*  
296     (Cnidaria, Hydrozoa, Siphonophorae, Cystonectae) from Brazil. *Iheringia, Sér. Zool.* 97 (4), 425–433.  
297     <https://doi.org/10.1590/S0073-47212007000400011>.
- 298     Bieri, R., 1959. Dimorphism and size distribution in *Velella* and *Physalia*. *Nature* 184, 1333–1334.  
299     <https://doi.org/10.1038/1841333a0>.
- 300     Canepa, A., Purcell, J.E., Córdova, P., Fernández, M., Palma, S., 2020. Massive strandings of pleustonic  
301     Portuguese Man-of-War (*Physalia physalis*) related to ENSO events along the southeastern Pacific Ocean.  
302     *Lat. Am. J. Aquat. Res.* 48 (5), 806–817. <https://doi.org/10.3856/vol48-issue5-fulltext-2530>.
- 303     Castelle, B., Marieu, V., Bujan, S., Splinter, K.D., Robinet, A., Sénéchal, N., Ferreira, S., 2015. Impact of  
304     the winter 2013–2014 series of severe Western Europe storms on a double-barred sandy coast: Beach and  
305     dune erosion and megacusp embayments. *Geomorphology* 238, 135–148.  
306     <https://doi.org/10.1016/j.geomorph.2015.03.006>.
- 307     Cavalcante, M.M.S., Rodrigues, Z.M.R., Hauser-Davis, R.A., Siciliano, S., Haddad Junior, V., Nunes, J.L.S.,  
308     2020. Health-risk assessment of Portuguese man-of-war (*Physalia physalis*) envenomations on urban  
309     beaches in São Luís city, in the state of Maranhão, Brazil. *Rev. Soc. Bras. Med. Trop.* 53, e20200216.  
310     <https://doi.org/10.1590/0037-8682-0216-2020>.
- 311     Cegolon, L., Heymann, W.C., Lange, J.H., Mastrangelo, G., 2013. Jellyfish stings and their management: A  
312     review. *Mar. Drugs* 11 (2), 523–550. <https://doi.org/10.3390/md11020523>.
- 313     Dudhat, S., Pande, A., Nair, A., Mondal, I., Srinivasan, M., Sivakumar, K., 2022. Spatio-temporal analysis  
314     identifies marine mammal stranding hotspots along the Indian coastline. *Sci. Rep.* 12, 4128.  
315     <https://doi.org/10.1038/s41598-022-06156-0>.
- 316     Ekman, V.W., 1905. On the influence of the Earth's rotation on ocean-currents. *Ark. Mat. Astron. Fys.* 2 (11),  
317     1–52.

318 Ferrer, L., González, M., Cotano, U., Uriarte, A., Sagarminaga, Y., Santos, M., Uriarte, Ad., Collins, M., 2004.  
319 Physical controls on the evolution of anchovy in the Bay of Biscay: A numerical approximation. ICES Ann.  
320 Sci. Conf., 22–25 September 2004, Vigo, Spain, ICES CM2004/P:07, 20 pp.

321 Ferrer, L., González, M., 2021. Relationship between dimorphism and drift in the Portuguese man-of-war.  
322 Cont. Shelf Res. 212, 104269. <https://doi.org/10.1016/j.csr.2020.104269>.

323 Ferrer, L., Pastor, A., 2017. The Portuguese man-of-war: Gone with the wind. Reg. Stud. Mar. Sci. 14, 53–62.  
324 <https://doi.org/10.1016/j.rsma.2017.05.004>.

325 Ferrer, L., Zaldua-Mendizabal, N., Del Campo, A., Franco, J., Mader, J., Cotano, U., Fraile, I., Rubio, A.,  
326 Uriarte, Ad., Caballero, A., 2015. Operational protocol for the sighting and tracking of Portuguese man-of-war  
327 in the southeastern Bay of Biscay: Observations and modeling. Cont. Shelf Res. 95, 39–53.  
328 <https://doi.org/10.1016/j.csr.2014.12.011>.

329 Francis, L., 1991. Sailing downwind: Aerodynamic performance of the *Velella* sail. J. Exp. Biol. 158 (1),  
330 117–132. <https://doi.org/10.1242/jeb.158.1.117>.

331 Hersbach, H., Bell, B., Berrisford, P., Biavati, G., Horányi, A., Muñoz Sabater, J., Nicolas, J., Peubey, C.,  
332 Radu, R., Rozum, I., Schepers, D., Simmons, A., Soci, C., Dee, D., Thépaut, J.-N., 2018. ERA5 hourly data  
333 on single levels from 1959 to present. Copernicus Climate Change Service (C3S) Climate Data Store (CDS).  
334 <https://doi.org/10.24381/cds.adbb2d47> (accessed on 14-Apr-2021).

335 Iosilevskii, G., Weihs, D., 2009. Hydrodynamics of sailing of the Portuguese man-of-war *Physalia physalis*. J.  
336 R. Soc. Interface 6 (36), 613–626. <https://doi.org/10.1098/rsif.2008.0457>.

337 Kendon, M., McCarthy, M., 2015. The UK’s wet and stormy winter of 2013/2014. Weather 70 (2), 40–47.  
338 <https://doi.org/10.1002/wea.2465>.

339 Kennedy, F.S., 1972. Distribution and abundance of *Physalia* in Florida waters. Florida Dept. Nat. Resour.,  
340 Mar. Res. Lab., Prof. Pap. Ser. 18, 38 pp.

341 Labadie, M., Aldabe, B., Ong, N., Joncquiert-Latarjet, A., Groult, V., Poulard, A., Coudreuse, M., Cordier, L.,  
342 Rolland, P., Chanseau, P., de Haro, L., 2012. Portuguese man-of-war (*Physalia physalis*) envenomation on  
343 the Aquitaine coast of France: An emerging health risk. Clin. Toxicol. 50 (7), 567–570.  
344 <https://doi.org/10.3109/15563650.2012.707657>.

345 Liu, Y., Weisberg, R.H., 2011. Evaluation of trajectory modeling in different dynamic regions using  
346 normalized cumulative Lagrangian separation. J. Geophys. Res. 116, C09013.  
347 <https://doi.org/10.1029/2010JC006837>.

348 Loten, C., Stokes, B., Worsley, D., Seymour, J.E., Jiang, S., Isbister, G.K., 2006. A randomised controlled  
349 trial of hot water (45 °C) immersion versus ice packs for pain relief in bluebottle stings. Med. J. Aust. 184  
350 (7), 329–333. <https://doi.org/10.5694/j.1326-5377.2006.tb00265.x>.

351 Louzao, M., Gallagher, R., García-Barón, I., Chust, G., Intxausti, I., Albisu, J., Brereton, T., Fontán, A., 2019.  
352 Threshold responses in bird mortality driven by extreme wind events. Ecol. Indic. 99, 183–192.  
353 <https://doi.org/10.1016/j.ecolind.2018.12.030>.

354 Macías, D., Prieto, L., García-Gorritz, E., 2021. A model-based management tool to predict the spread of  
355 *Physalia physalis* in the Mediterranean Sea. Minimizing risks for coastal activities. Ocean Coast. Manag. 212,  
356 105810. <https://doi.org/10.1016/j.ocecoaman.2021.105810>.

357 Maharani, T., Widiastuti, W., 2021. First envenomation report of the Cnidarian *Physalia physalis* in Indonesia.  
358 Int. Marit. Health 72 (2), 110–114. <https://doi.org/10.5603/IMH.2021.0019>.

359 Mapstone, G.M., 2014. Global diversity and review of Siphonophorae (Cnidaria: Hydrozoa). PLoS ONE 9 (2),  
360 e87737. <https://doi.org/10.1371/journal.pone.0087737>.

361 Morley, T.I., Fayet, A.L., Jessop, H., Veron, P., Veron, M., Clark, J., Wood, M.J., 2016. The seabird wreck in  
362 the Bay of Biscay and Southwest Approaches in 2014: A review of reported mortality. Seabird 29, 22–38.

363 Munro, C., Vue, Z., Behringer, R.R., Dunn, C.W., 2019. Morphology and development of the Portuguese man  
364 of war, *Physalia physalis*. Sci. Rep. 9, 15522. <https://doi.org/10.1038/s41598-019-51842-1>.

365 Orton, J.H., 1913. The occurrence of the Portuguese man-of-war (*Physalia*), and of a giant spider-crab,  
366 “*Homola (Paromola) cuvieri*,” in the English Channel. Nature 90, 700. <https://doi.org/10.1038/090700a0>.

367 Priestley, M.D.K., Pinto, J.G., Dacre, H.F., Shaffrey, L.C., 2017. The role of cyclone clustering during the  
368 stormy winter of 2013/2014. Weather 72 (7), 187–192. <https://doi.org/10.1002/wea.3025>.

369 Prieto, L., Macías, D., Peliz, A., Ruiz, J., 2015. Portuguese Man-of-War (*Physalia physalis*) in the  
370 Mediterranean: A permanent invasion or a casual appearance? Sci. Rep. 5, 11545.  
371 <https://doi.org/10.1038/srep11545>.

372 Savilov, A.I., 1961. The distribution of the ecological forms of the by-the-wind sailor, *Veleva lata* Ch. and Eys.,  
373 and the Portuguese man-of-war, *Physalia utriculus* (La Martinière) Esch., in the North Pacific. Tr. Inst.  
374 Okeanol. Akad. Nauk SSSR 45, 223–239.

375 Shannon, L.V., Chapman, P., 1983. Incidence of *Physalia* on beaches in the South Western Cape Province  
376 during January 1983. S. Afr. J. Sci. 79 (11), 454–458.

377 Sibley, A., Cox, D., Titley, H., 2015. Coastal flooding in England and Wales from Atlantic and North Sea storms  
378 during the 2013/2014 winter. Weather 70 (2), 62–70. <https://doi.org/10.1002/wea.2471>.

379 Skamarock, W.C., Klemp, J.B., Dudhia, J., Gill, D.O., Liu, Z., Berner, J., Wang, W., Powers, J.G., Duda, M.G.,  
380 Barker, D.M., Huang, X.-Y., 2021. A description of the Advanced Research WRF Model Version 4. NCAR  
381 Technical Note, NCAR/TN-556+STR, 148 pp. <https://doi.org/10.5065/1dfh-6p97>.

382 Thompson, V., Dunstone, N.J., Scaife, A.A., Smith, D.M., Slingo, J.M., Brown, S., Belcher, S.E., 2017. High  
383 risk of unprecedented UK rainfall in the current climate. Nat. Commun. 8, 107.  
384 <https://doi.org/10.1038/s41467-017-00275-3>.

385 Totton, A.K., Mackie, G.O., 1956. Dimorphism in the Portuguese man-of-war. Nature 177, 290.  
386 <https://doi.org/10.1038/177290b0>.

387 Totton, A.K., Mackie, G.O., 1960. Studies on *Physalia physalis* (L.). Part 1. Natural History and Morphology.  
388 Part 2. Behaviour and Histology. Discovery Reports 30, 301–408.

389 Truchon, M.-H., Measures, L., L'Hérault, V., Brêthes, J.-C., Galbraith, P.S., Harvey, M., Lessard, S., Starr,  
390 M., Lecomte, N., 2013. Marine mammal strandings and environmental changes: A 15-year study in the St.  
391 Lawrence ecosystem. PLoS ONE 8 (3), e59311. <https://doi.org/10.1371/journal.pone.0059311>.

392 Wilcox, C.L., Yanagihara, A.A., 2016. Heated debates: Hot-water immersion or ice packs as first aid for  
393 Cnidarian envenomations? Toxins 8 (4), 97. <https://doi.org/10.3390/toxins8040097>.

394 Wilson, D.P., 1947. The Portuguese man-of-war *Physalia physalis* L., in British and adjacent seas. J. Mar.  
395 Biol. Assoc. U.K. 27 (1), 139–172. <https://doi.org/10.1017/S0025315400014156>.

396 Woodcock, A.H., 1956. Dimorphism in the Portuguese man-of-war. Nature 178, 253–255.  
397 <https://doi.org/10.1038/178253a0>.

398 Woodcock, A.H., 1971. Note concerning *Physalia* behavior at sea. Limnol. Oceanogr. 16 (3), 551–552.  
399 <https://doi.org/10.4319/lo.1971.16.3.0551>.

400 Woodcock, A.H., 1997. Why sailing sea animals have mirror images. *Pac. Sci.* 51 (1), 12–17.

401

402 **Figure captions**

403 **Fig. 1.** Sailing directions of right- and left-handed *P. physalis*.

404

405 **Fig. 2.** Prototypes of right- and left-handed *P. physalis* (top) and components of the satellite-tracked surface  
406 drifting buoys used in this study (bottom).

407

408 **Fig. 3.** Two-day trajectories obtained from an initial example trajectory.

409

410 **Fig. 4.** General surface ocean circulation in the North Atlantic Subtropical Gyre. The black triangle indicates  
411 the initial location (42.2° N, 8.9° W) of the 2014 PMW swarm in the SOFT simulations where time ran  
412 backwards.

413

414 **Fig. 5.** Trajectories of four satellite-tracked surface drifting buoys (from top left to bottom right: 20170517,  
415 20180222, 20190320 and 20210920). The black triangles and circles indicate the initial and final GPS  
416 locations of the buoys, respectively.

417

418 **Fig. 6.** Simulated trajectories of the 2014 PMW swarm (from 11 February 2014 to 1 September 2013, both  
419 dates at 12:00 UTC) obtained with SOFT using a wind drag coefficient of 0.04 and negative and positive  
420 drift angles (top and bottom, respectively). The black triangle and circles indicate the initial and final  
421 locations of the swarm in the SOFT simulations, respectively.

422

423 **Fig. 7.** As in Fig. 6, but using a wind drag coefficient of 0.02.

424

425 **Fig. 8.** As in Fig. 6, but using a wind drag coefficient of 0.06.

426

427 **Fig. 9.** Low-density prototypes of right- and left-handed *P. physalis* made from air bags for packaging and  
428 wool yarns.

429 **Table captions**

430 **Table 1**

431 Drift periods and initial and final GPS locations of the 27 satellite-tracked surface drifting buoys used in this  
432 study.

Buoy ID	Initial and final dates (day/month/year) and times (UTC)	Initial and final GPS locations
20150517A	17/05/2015 09:54:22–13/06/2015 12:13:01	45.45° N, 4.21° W–43.44° N, 4.06° W
20150517B	17/05/2015 10:58:54–16/06/2015 09:44:36	45.63° N, 4.21° W–43.44° N, 2.95° W
20150926	26/09/2015 00:41:54–25/10/2015 00:26:37	45.88° N, 4.69° W–46.02° N, 8.59° W
20151025	25/10/2015 19:19:36–06/11/2015 11:38:34	46.22° N, 8.61° W–48.31° N, 8.81° W
20160321A	21/03/2016 02:48:12–04/04/2016 23:52:05	46.26° N, 4.28° W–46.47° N, 3.1° W
20160321B	21/03/2016 05:14:35–11/04/2016 05:02:25	46.25° N, 4.75° W–46.23° N, 1.87° W
20160321C	21/03/2016 08:28:59–11/04/2016 05:50:36	46.25° N, 5.26° W–46.62° N, 2.68° W
20160321D	21/03/2016 22:17:58–05/04/2016 00:19:53	46.76° N, 5.77° W–47.65° N, 3.51° W
20160322	22/03/2016 02:25:22–04/04/2016 00:10:08	46.77° N, 5.26° W–47.79° N, 3.83° W
20160519A	19/05/2016 07:13:35–16/06/2016 20:39:23	45.87° N, 4.21° W–43.79° N, 1.42° W
20160519B	19/05/2016 09:08:05–28/06/2016 10:41:23	46.12° N, 4.38° W–43.84° N, 2.01° W
20160709	09/07/2016 07:07:06–01/08/2016 12:12:53	45° N, 3.36° W–43.55° N, 5.55° W
20160923	23/09/2016 15:35:06–13/11/2016 19:14:07	45.78° N, 4.2° W–44.64° N, 8.7° W
20170517	17/05/2017 13:30:07–30/06/2017 14:17:28	45.87° N, 3.71° W–43.49° N, 3.83° W
20180222	22/02/2018 21:58:52–04/04/2018 08:57:26	45.5° N, 4.03° W–46.63° N, 1.89° W
20180224	24/02/2018 11:20:40–31/03/2018 23:42:58	45.5° N, 4.38° W–46.53° N, 1.83° W
20180225	25/02/2018 03:18:37–04/04/2018 06:25:25	45.51° N, 4.19° W–46.65° N, 1.91° W
20180226	26/02/2018 23:17:06–14/03/2018 23:50:23	45.5° N, 3.86° W–47.49° N, 2.83° W
20180515	15/05/2018 03:51:09–21/05/2018 10:14:56	44.86° N, 2.84° W–44.23° N, 3.01° W
20190320	20/03/2019 15:56:58–24/04/2019 11:18:27	46.25° N, 4.18° W–45.72° N, 5.96° W
20190409	09/04/2019 15:32:57–12/04/2019 09:17:23	46° N, 4.01° W–45.75° N, 4.21° W
20190418	18/04/2019 22:14:07–27/04/2019 20:23:26	46° N, 4.02° W–46.13° N, 2.75° W
20200918	18/09/2020 16:06:42–26/09/2020 16:27:57	44.67° N, 3.04° W–44.2° N, 1.3° W
20210513	13/05/2021 08:10:26–23/05/2021 07:54:59	45.62° N, 4.13° W–45.64° N, 1.1° W
20210919	19/09/2021 20:06:19–25/11/2021 00:57:35	45.77° N, 4.17° W–43.46° N, 3.95° W
20210920	20/09/2021 12:16:23–27/11/2021 05:42:57	45.93° N, 4.55° W–43.44° N, 4.1° W
20220515	15/05/2022 11:20:40–13/06/2022 18:02:27	45.13° N, 3.63° W–43.58° N, 5.74° W

433